

Optimized detection of phase amplified light for imaging resolution improvement

Y.C. Yin · I. Jovanovic

Received: 8 August 2011 / Revised version: 20 January 2012 / Published online: 21 April 2012
© Springer-Verlag 2012

Abstract The use of quantum phase amplification has been proposed to enhance the spatial resolution of imaging systems. A key component of this approach is the production of phase-amplified light, which can be generated in a phase-sensitive three-wave nonlinear mixing process, such as an optical parametric amplifier. Here we present a refined model for detection of phase-amplified light produced by this method, which includes optimization of detector segmentation, detector noise, and detection in both the spatial and the spatial frequency domain. The implications of quantum phase amplification for resolution of optical imaging are considered in a canonical imaging resolution problem.

1 Introduction

The classical limit on the resolution of optical imaging systems is determined by the aperture size (D) and the wavelength (λ), and is referred to as the Rayleigh criterion:

$$\theta_{\min} \geq \theta_R = 1.22\lambda/D, \quad (1)$$

where θ_{\min} is the minimum resolvable angle and θ_R is the Rayleigh angle. However, increasing the optical aperture size can be costly, and the use of shorter wavelengths can be impractical or limited by effects such as opacity. Various techniques for overcoming the classical resolution limit to achieve *super-resolution* with coherent light sources

have been proposed, such as point-spread function engineering [1, 2], structured illumination [3], off-axis illumination [4], and localization microscopy [5]. In this paper, we numerically analyze several important aspects of the performance of quantum phase amplification (QPA), a novel approach for achieving super-resolution.

QPA has been previously proposed [6, 7] as a method to perform nonclassical manipulation of coherent light. QPA can be experimentally realized by using nonlinear optical mixing processes, of which phase-sensitive three-wave mixing (PSTWM) is one convenient choice [8]. PSTWM is known to produce squeezed states of electromagnetic field, and is typically used to amplify the signal without imparting additional noise [9]. QPA occurs when PSTWM is operated in the photon number deamplification mode, i.e., when the energy is coherently transferred from the low-frequency signal wave to the high-frequency pump wave. The final state is nonclassical, with the field amplitude squeezed and the phase antisqueezed. If the small-signal deamplification gain coefficient is denoted by g , the field transformation occurring in the ideal QPA process is [6]

$$E \exp(i\varphi) \rightarrow E/\sqrt{g} \exp(ig\varphi), \quad (2)$$

where E is the amplitude of the incident electric field, and φ corresponds to the departure of the phase relationship among the input pump, signal, and idler waves from the ideal deamplification condition:

$$\varphi = \phi_3(0) - \phi_2(0) - \phi_1(0) - \pi/2. \quad (3)$$

In Eq. (3), the phases of the signal, idler, and pump at the amplifier input are denoted by $\phi_1(0)$, $\phi_2(0)$, and $\phi_3(0)$, respectively.

In our prior work, we have developed a semiclassical model for QPA implemented by PSTWM, both in the temporal and the spatial domain, and discussed its features and

Y.C. Yin · I. Jovanovic (✉)
Department of Mechanical and Nuclear Engineering,
The Pennsylvania State University, University Park, PA 16802,
USA
e-mail: ijovanovic@psu.edu
Fax: +1-814-8636382

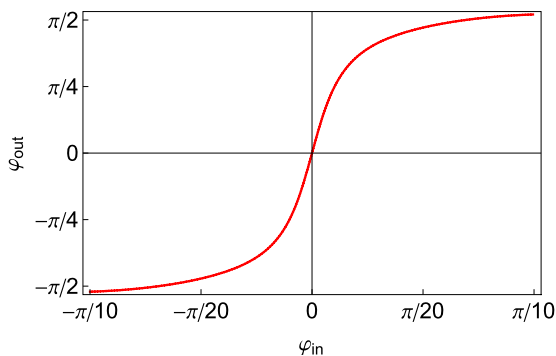


Fig. 1 An example for phase amplification characteristic $\varphi_{out} = f(\varphi_{in})$ calculated for PSTWM with undepleted pump [11]. The characteristic is linear for a small output phase difference among the signal, idler, and pump ($\varphi_{out} \ll \pi/2$)

possible applications. For example, it has been shown that QPA can be applied in the temporal domain to generate a controllable phase modulation, which can result in pulse compression, pulse steepening, or generation of pulse doublets and pulse trains [10]. In the spatial domain, it has been shown that QPA can amplify the phase distribution transverse to beam propagation, which can be used to improve the imaging resolution [11–14]. The phase amplification process can be described using the phase amplification characteristic $\varphi_{in} = f(\varphi_{out})$, where φ_{in} and φ_{out} are the departures of the signal-idler-pump phase relationship from the ideal deamplification condition, as defined in Eq. (3), at the input and the output of the amplifier, respectively. As shown in Fig. 1, within a limited range of phase in the neighborhood of the ideal phase condition ($\varphi = 0$), φ_{out} is nearly a linear function of φ_{in} , i.e., $\varphi_{out} \approx g\varphi_{in}$.

Here we report a significant extension of our previously developed model for resolution improvement by use of QPA in the spatial domain. We focus on the detection of phase amplified light and provide strategies for the optimization of the signal-to-noise ratio (SNR) that take advantage of both the change of the field distribution and the change of energy of the signal in the QPA process. Specifically, the features of the present discussion that were not present in our prior work on the resolution improvement using QPA include: (i) implementation of a realistic detector noise model, (ii) optimization of detector segmentation, and (iii) consideration of detection of the signal both in the spatial and the spatial frequency domains. A discussion of these important characteristics of this novel approach to resolution improvement is presented, with additional insight provided by appropriate examples.

2 Principles of QPA-enhanced imaging

The physical mechanism for imaging resolution enhancement via QPA is conceptually illustrated in Fig. 2. For sim-

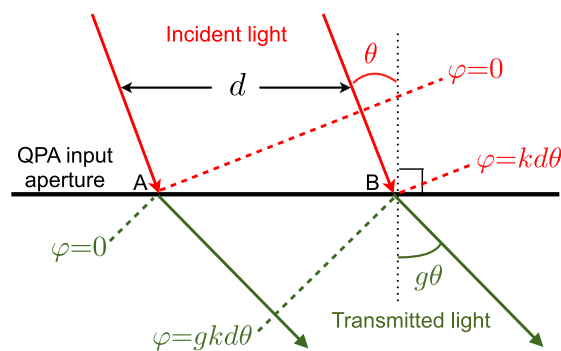


Fig. 2 Conceptual representation of an ideal QPA, which increases the apparent angle of incidence of a plane wave θ on the QPA aperture by a factor of g to $g\theta$. The apparent angle of incidence of the beam is amplified without the change in beam divergence. The reference phase coincides with the QPA input aperture and is not shown

plicity of this discussion and the ease of future implementation, here we consider only a degenerate type I three-wave mixing process, in which the signal and the idler beams are identical. A plane wave signal is incident on the input aperture of the quantum phase amplifier at an angle θ relative to the direction normal to the aperture. Another plane wave (pump, not shown for clarity) is incident perpendicular to the same aperture and sets the reference phase. The relative phase between the signal and the pump varies linearly across the amplifier aperture. After phase amplification with a gain $g > 1$, at the output aperture of the quantum phase amplifier the relative phase between the signal and the reference beam (pump) increases by a factor of g , resulting in the transmitted signal angle being $g\theta$. This increase in the transmitted angle is equivalent to the incidence of the signal onto the amplifier at a greater angle. Unlike a telescope (lens) which can also change the beam angle, in QPA this angular amplification is not accompanied by the increase in the width of the spatial frequency spectrum, and can thus lead to an improvement of the imaging resolution. The minimum resolving angle for a classical imaging system following ideal QPA becomes $\sim \lambda/(gD)$.

Near-ideal QPA can be experimentally realized by the use of nonlinear optical processes. For example, it has been shown [11] that PSTWM exhibits the required properties for QPA, as expected given its related application in quantum optics for generation of squeezed states of light. The use of PSTWM for QPA in the spatial domain is subject to certain constraints. The important criteria for operation of PSTWM commensurate with resolution-enhancing QPA include the finite size of the aperture (non-vanishing width of the transverse spatial frequency spectrum), the requirement on the incidence signal angle to be smaller than the Rayleigh angle θ_R , and the restriction of the gain to produce a maximum amplified angle around the Rayleigh angle [11].

The design for a proof-of-principle experiment that would demonstrate the angular amplification of the input

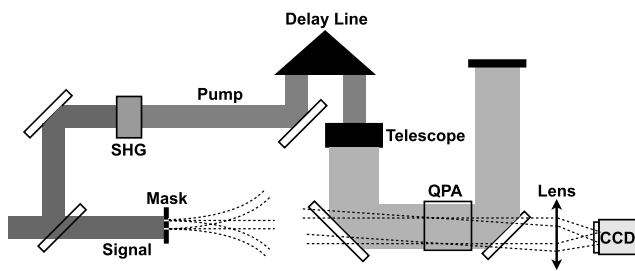


Fig. 3 Simplified design for a proof-of-principle experiment to demonstrate QPA in the spatial domain. QPA utilizes a pump beam produced by second-harmonic generation of the 800-nm pulse split from the same laser. A 1-mm diameter pump beam sets the effective Rayleigh angle of the system to 1 mrad. Two holes with 100- μm separation are illuminated by a laser to produce two point-like sources. The distance between the mask and the quantum phase amplifier is set to 10 m, resulting in the source angular separation of $\theta_R/100$. QPA is detected by measuring the modification of the far field distribution and the power of the signal beam when the pump beam is present and when it is blocked

signal in QPA is shown in Fig. 3. The design parameters are consistent with the ones used in the numerical simulations discussed in Sects. 4–6, and the laser characteristics are chosen to be readily available from standard laser systems. A 800-nm pulse is split into the signal beam and the beam used to generate pump. The pump at 400 nm is generated by second-harmonic generation from the same laser, which ensures that coherence exists between the pump and the signal. Since the phase gain coefficient is proportional to the product of crystal length and the root square of pump intensity, the important parameters for determining QPA gain are the pump intensity and the crystal length. For example, if a 1.6-mm long BBO crystal is used for QPA, the pump intensity in the range of 10 GW/cm^2 is required to produce a phase gain of order 100. The angle between the pump and the signal is chosen to be $\theta_R/100$. Phase-sensitive operation is established by the use of a precision delay line. The effect of QPA can be measured by the analysis of the far field and is expected to be manifested as the change of the centroid and the distribution of the far field.

3 Quantification of resolution by information theory

The imaging resolution problem considered here is treated as a binary hypotheses testing problem, illustrated in Fig. 4. In hypothesis 1, a single point source is present and located on the axis of the imaging system, while in hypothesis 2, two point sources are present, with one located on-axis and the other located at a small off-axis angle. In our analysis, the intensity produced by the point source in hypothesis 1 is twice that of the individual point source in hypothesis 2, yielding identical energy incident on the imaging system for both hypotheses. A standard approach to addressing the distinguishability problem (associating the measured data with

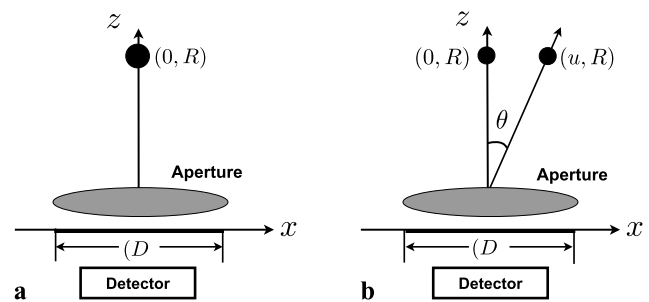


Fig. 4 The definition of (a) hypothesis 1: a point source at $(0, R)$; (b) hypothesis 2: two point sources located at $(0, R)$ and (u, R) with a separation angle θ

one of the two available hypotheses) is calculating the SNR as defined by Helstrom [15]. The hypothesis 1 is associated with illuminance J_0 , which is due to one point source and background, while the hypothesis 2 is associated with illuminance J_1 , which is due to two point sources and background. Here we use the likelihood SNR, which applies to the case when the signals are stronger or comparable to the background:

$$\text{SNR} = \frac{\int M(x) \ln[M_1(x)/M_0(x)] dx}{\int M_0(x) \ln^2[M_1(x)/M_0(x)] dx}, \tag{4}$$

where $M(x)$ is the difference between expected count-rate densities for two hypotheses:

$$M(x) = M_1(x) - M_0(x). \tag{5}$$

4 Detection in the spatial and the spatial frequency domain

The light incident onto the aperture of an imaging system can be fully described by the use of complex electric field $\mathbf{E}(\mathbf{r})$, or its Fourier conjugate $\mathbf{E}(\mathbf{k})$. A complete measurement of the electric field can be achieved by the use of homodyne detection, effectively projecting the complex field \mathbf{E} onto the two complex quadrature axes. In practice, such detection method is significantly more complex than a simple measurement of the intensity distribution $|\mathbf{E}(\mathbf{r})|^2$ or $|\mathbf{E}(\mathbf{k})|^2$, which can be achieved by imaging or focusing the collected signal onto a simple detector and measuring the produced photocurrent. This is especially convenient in scenarios in which pulsed, single-shot detection is needed.

It is inevitable that some information is lost in the measurement in which only the amplitude of the complex field is captured. As a result, it is expected that such suboptimal detection methodology will exhibit SNR lower than that achievable if a complete field measurement is made. In this case of the use of an incomplete, but relatively common, method to measure the electric field, QPA has a potential to

offer significant improvement in SNR when implemented in an imaging system.

Improvement of distinguishability by the use of QPA can be intuitively understood by considering the transformation performed on the field distribution in both the spatial frequency and the spatial domains. We introduce a convenient normalization of the angular and spatial scales used to represent the field distributions. In the case of the angular distribution, the angle is normalized to the Rayleigh angle. We refer to this distribution as “spatial frequency distribution”, as the adopted normalized angular scale is linear in transverse spatial frequency, i.e., simply rescaled spatial frequency distribution. The spatial distribution is normalized to the aperture diameter (D), and we similarly also refer to the distribution on a dimensionless scale as “spatial distribution”.

We first illustrate this for an ideal QPA, described by Eq. (2), where it can be easily seen that the distinguishability depends on whether the measurement is performed in the spatial or the spatial frequency domain. In the example of an ideal QPA, shown in Fig. 5, we use the previously introduced binary hypotheses problem (Fig. 4), in which the phase gain is assumed to be 100, and the initial angular separation between the two point sources in hypothesis 2 is $\theta_R/100$. In the spatial frequency domain, the initial intensity distributions before QPA for the hypothesis 1 (dotted thin line) and the hypothesis 2 (solid thin line) are overlapped and cannot be readily distinguished. This is because the angular separation ($\theta_R/100$) between the two point sources in hypothesis 2 is significantly below the Rayleigh limit and thus the two point sources appear as one point source. After QPA, the energy of the point source in hypothesis 1 is deamplified with no concomitant shift in the spatial frequency spectrum, as shown by thick dotted line in Fig. 5(a). In hypothesis 2 after QPA, the angular separation (the separation of the two peaks shown in Fig. 5(a) and indicated by solid thick line) between the two point sources is amplified from $\theta_R/100$ to θ_R . This angle amplification is due to phase variation defined by Eq. (3) across the aperture surface. Therefore, it can be seen that the application of QPA helps to distinguish the two hypotheses in the spatial frequency domain. In the spatial domain shown in Fig. 5(b), the intensity distributions for the two hypotheses cannot be distinguished after QPA because the two hypotheses experience an equal photon number deamplification gain.

We next consider distinguishability improvement in the same binary hypotheses problem by using a real QPA realized by PSTWM. We do this formally by performing an example calculation with the following parameters. The off-axis incidence angle is $\theta_R/100$, the signal/idler has a wavelength of 800 nm with the intensity set to 0.5 GW/cm^2 , and the incident pump has a wavelength of 400 nm with an intensity of 10 GW/cm^2 . PSTWM is realized in a β -barium borate (BBO) crystal with a length of 1.6 mm, resulting in

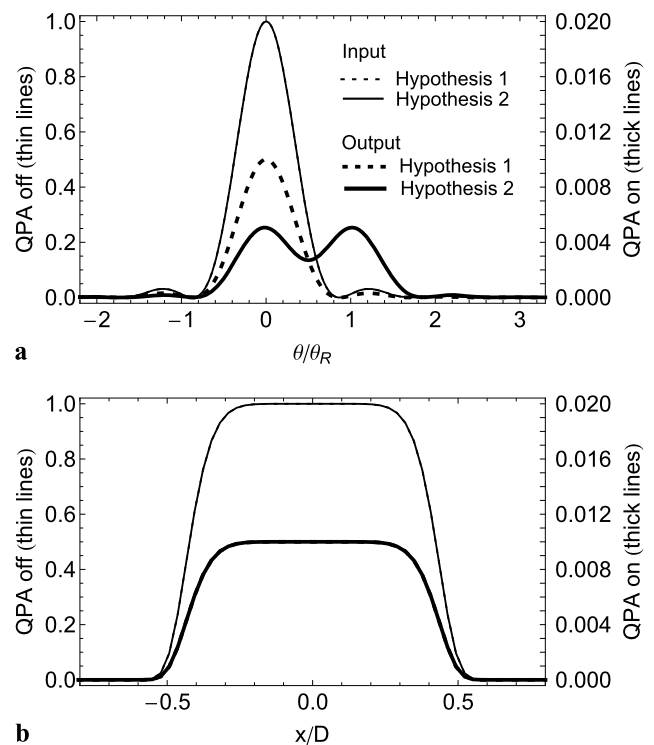


Fig. 5 Ideal QPA transformation of the transverse intensity distribution in (a) spatial frequency and (b) spatial domain for the previously introduced hypotheses (Fig. 4). The input intensity distributions for the two hypotheses are well overlapped and thus not distinguishable. The angular and the spatial domain scales have been normalized to the Rayleigh angle (θ_R) and the aperture diameter (D), respectively. In the spatial domain, the output intensity distributions for the two hypotheses are also overlapped

the photon number deamplification gains for hypotheses 1 and 2 being 26 and 66, respectively. The numerical model used for this calculation has been previously described [11]. The resulting distributions in the spatial frequency domain and the spatial domain are shown in Fig. 6. In the spatial frequency domain, the intensity distributions before QPA for the hypothesis 1 (dotted thin line) and the hypothesis 2 (solid thin line) are overlapped due to their small angular separation. After QPA, the distribution associated with hypothesis 1 is deamplified with no concomitant shift in the spatial frequency spectrum (albeit with some reshaping), as shown by thick dotted line in Fig. 6(a). The hypothesis 2 is considerably reshaped and can be readily distinguished from hypothesis 1, although it can be seen that an intuitive picture involving the increase of peak separation in the spatial frequency domain is not as clearly manifested in real QPA implemented by PSTWM (which is limited to angles much smaller than the Rayleigh angle). We note that this does not reduce the distinguishability and utility of the approach, however, as can be demonstrated rigorously by the use of SNR. In the spatial domain shown in Fig. 6(b), the intensity distributions for the two hypotheses cannot be distinguished

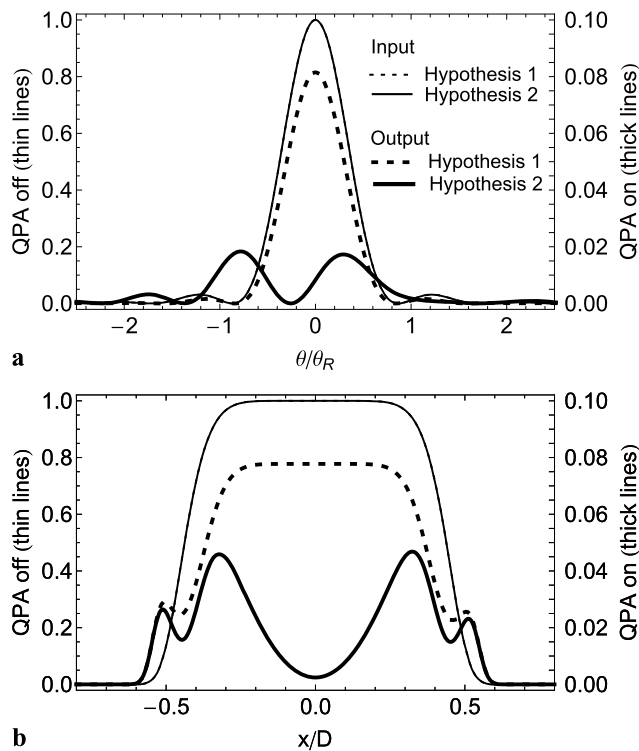


Fig. 6 Transformation of the transverse intensity distribution performed in QPA implemented by PSTWM in (a) spatial frequency and (b) spatial domain for the previously introduced hypotheses (Fig. 4). The input intensity distributions for the two hypotheses are well overlapped and thus not distinguishable. The angular frequency and the spatial domain scales have been normalized to the Rayleigh angle (θ_R) and the aperture diameter (D), respectively

before QPA and are distinguished after QPA by comparing the shape of their distributions, or by simply measuring their energies, since they experience different photon number deamplification gains in QPA.

It is not immediately evident that the modification of the spatial frequency distribution is more observable compared to that of the spatial distribution. However, this is confirmed by a formal calculation of the SNR defined by Eq. (3) for both the far-field distribution $|\mathbf{E}(\mathbf{k})|^2$ and the near-field distribution $|\mathbf{E}(\mathbf{r})|^2$ (Fig. 7). For this calculation, the gain increase is achieved by increasing the BBO crystal length, while all other parameters are the same as those used in Fig. 6. Without QPA, the SNR is essentially zero because the spatial frequency distributions are very similar and energies are identical. When the QPA is applied, the SNR increases with gain in both the spatial frequency and the spatial domains, since the distributions for the two hypotheses are modified at different rates. It is found that SNR calculated in the spatial frequency domain is always higher than that in the spatial domain.

To summarize, when using a simple intensity or intensity distribution measurement in a non-ideal QPA realized by PSTWM, two important observations can be made:

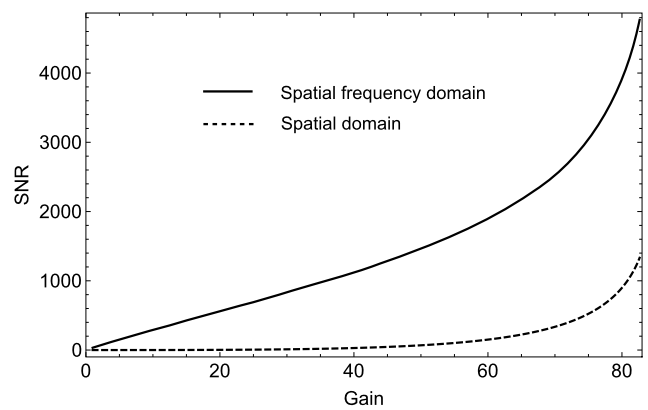


Fig. 7 SNR for the two hypotheses shown in Fig. 4 when the measurement is performed in the spatial frequency domain (solid) and the spatial domain (dotted)

1. Since QPA exhibits different gains for two different incident distributions, a simple measurement of the total power can be used to distinguish the two hypotheses, which is not possible without QPA. The result of this measurement is independent on whether it is made in the spatial or the spatial frequency representation of the field.
2. While the two electric field representations $\mathbf{E}(\mathbf{r})$ and $\mathbf{E}(\mathbf{k})$ are equivalent to each other both prior to and following the QPA, the simple measurement of the intensity distribution $|\mathbf{E}(\mathbf{r})|^2$ or $|\mathbf{E}(\mathbf{k})|^2$ can yield significant differences in distinguishability. This is because the modification of the electric field distribution under action of QPA can be of different magnitude, depending on whether it is measured in the spatial or the spatial frequency domain.

Thus in the absence of the optimal detector that captures the complete information on the complex electric field \mathbf{E} , the use of QPA can offer a significant improvement of SNR, but the choice of performing detection in the spatial or the spatial frequency domain has to be made judiciously and it depends on the specific scenario. In the problem of sub-Rayleigh imaging considered here, detection in the spatial frequency domain appears to be preferred.

5 Detector noise and segmentation

Two critical aspects of the detection process not included in the previous discussion are the presence of detector noise and the finite detector segmentation. They are considered here in more detail in an effort to arrive with a more comprehensive set of design principles needed to take advantage of the unique properties of the QPA process for resolution improvement.

The primary contributions to the noise in the detection process are the shot noise associated with the discrete nature

of the collected photon signal and the dark current noise associated with the detector itself. The shot noise can be modeled as a Poissonian process and is already included in the formal calculation of SNR (Eq. (3)). The dark current originating from thermal generation in the detector can be similarly modeled as a Poissonian process, and its contribution to the total noise needs to be included in the SNR calculation.

The other important consideration is the detector segmentation, which affects the sampling of the incident signal. In conjunction with this feature of the detector, we note that:

1. An important feature of the transformation performed by QPA is the modification of the electric field distribution, increasing the difference between the two similar distributions incident onto the QPA. Ability to resolve the distribution shape is thus expected to result in a greater SNR than a simple measurement of energy.
2. Assuming the ability of the imaging system following the QPA to resize the beam to any convenient size, the convenient scale for quantifying the detector segmentation is the ratio of beam size to detector pixel size.
3. While the reduction of detector segment size allows for ever finer sampling and better distinction between different spatial distributions, the trade-off is the reduction of the intensity of signal striking individual detector segments, resulting in a lower SNR on each detector segment.

Thus the consideration of detector segmentation is intertwined with the noise analysis. To the first order, a simple assumption can be made in the subsequent analysis that the magnitude of detector noise is independent of the detector segment size. In this case, the trade-off in the choice of detector segmentation is apparent, as the increase in the detector segment size increases the amount of signal compared to the detector noise on each segment, but details of the distribution are progressively less accessible with coarse sampling. Again, the choice of detector segmentation is problem-specific, but we provide a convenient example that illustrates the key design principles.

We parametrize the following calculation in terms of the ratio of the beam size and the detector segment (pixel) size, with beam size defined as the full-width-half-maximum of a Gaussian beam. The calculation is performed for the previously introduced scenario shown in Fig. 6, considering only the far-field (spatial frequency) distribution. The signal is assumed to be shot-noise limited, and a Poissonian background noise is added to the signal, arising from the dark current noise associated with the detector. A typical dark current equivalent to 2500 photons/pixel is chosen, resulting in the Poissonian fluctuation of the dark current being 2%. For this example, the BBO crystal length is chosen to be 1.2 mm and the resulting SNR is calculated for two characteristic cases:

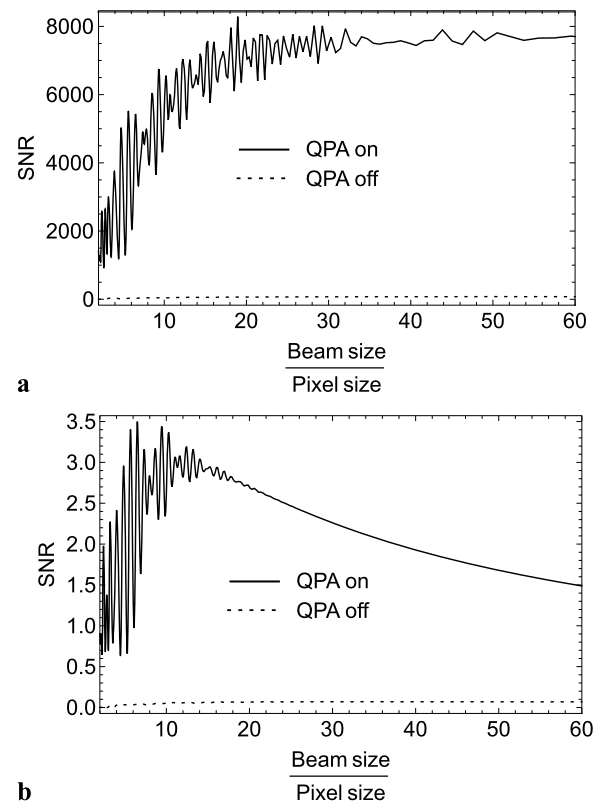


Fig. 8 Effect of the segmentation on the SNR: (a) large signal compared to dark current; (b) small signal comparable to dark current

1. Large signal to background ratio. A total of 3.0×10^9 photons corresponding to an intensity of 4.5×10^7 W/cm² are incident onto QPA, resulting in 3.3×10^7 photons following the QPA and incident onto the detector. For the case of 100 detector segments, this corresponds to the signal to dark current ratio of 132, clearly in the regime in which the dark current is negligible compared to the incident signal.
2. Low signal to noise ratio. The number of photons incident onto the QPA and the detector is 3.0×10^6 (corresponding to an intensity of 4.5×10^4 W/cm²) and 3.4×10^4 , resulting in the signal power equivalent to dark current power when the ratio of beam size to detector segment size is 10.

The results of the calculation pertaining to these two characteristic cases are shown in Fig. 8. For the case 1, as the detector pixel size is decreased, the improved sampling of the intensity distribution allows the difference between the two hypotheses to be determined with a greater accuracy, with little penalty due to reduced signal photon number on each detector pixel. As the detector segment size is being reduced, some oscillatory variation of SNR occurs as the sampling becomes comparable to the characteristic size of the features of the distribution. In this example, the SNR reaches its maximum when the detector segment size is set

to approximately 1/30 of the beam size, as the pixel size is fine enough to capture the intensity distribution profiles for the two hypotheses.

However, in the case 2, when the signal is comparable to the dark current, the SNR first increases with decreasing detector segment size as the important features of the distribution are captured. The SNR reaches a maximum when the detector size is set to approximately 1/10 of the beam size. As the detector segment size decreases further, SNR begins to decrease due to the increased effect of dark current and its competition with the signal. Thus the detector segmentation has to be carefully chosen to optimize the SNR, with the importance of this optimization increasing when QPA is used.

6 Application of QPA in imaging systems

The proposed approach for the use of QPA in an imaging system is illustrated in Fig. 9. Two characteristic rays (on-axis and off-axis) originating from a distant object illuminated by coherent light are shown. The rays are collected by an aperture and resized by a telescope T to a convenient size for QPA enhancement. This results in rescaling of angles associated with the incoming rays, and a transverse gradient of relative phase between the signal and the pump is established on the input aperture of QPA. The QPA amplifies the spatial variations of phase of the signal incident on the amplifier, increasing the apparent angular separation between the on-axis and the off-axis rays. The phase-amplified light is transported to the detector using a transport optical system (in this example, lens L). The transport optical system can image either the near or the far field of the signal onto the detector. The detector is a simple segmented detector that records the photocurrent proportional to the number of photons striking each detector segment.

We finally consider some additional important practical aspects of the proposed approach to the application of QPA in imaging systems.

1. *Imaging range.* This is an active imaging technique that requires illumination of the object by coherent light, its collection, and imaging onto the quantum phase amplifier. Assuming that the illumination can be achieved by focusing the laser light onto a small region of interest, the diffuse nature of reflection can be assumed to dominate the losses and determine the minimum energy and maximum range for which the technique is applicable. For example, in Fig. 10, we consider the illumination of an object at a 10 km range with a 10 cm spot size using a laser with a wavelength of 1 μm . Assuming a 50 % transmission loss and 50 % target reflectivity, as well as the isotropic diffuse emission from the object into a 2π solid angle, a 2 mJ transmitter pulse is needed to collect

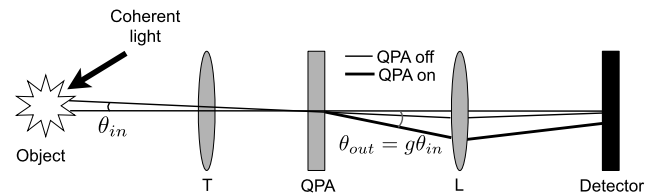


Fig. 9 Integration of the QPA into a simple imaging system. A telescope T can be used to resize the beam from the collection aperture to a convenient size for QPA enhancement. The lens L is used to transport the QPA-enhanced beam for measurement either in the near field or the far field. An incident off-axis ray emerges from the QPA at a greater angle (*thick*) when the QPA is pumped compared to propagating without angular change when QPA is inactive (*thin line*)

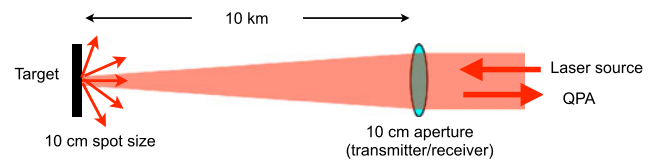


Fig. 10 A practical active imaging scenario over 10 km distance with 10 cm aperture

10^4 photons from a 1-cm diameter sub-Rayleigh region of the illuminated object and collect the light by a 10-cm aperture. This is clearly not a demanding energy requirement. In practice, effects such as atmospheric absorption and turbulence will affect the energy and phase characteristics of the received signal. Those effects could be mitigated by the use of appropriate wavelength and by the use of adaptive optics, respectively.

2. *Coherence.* The use of QPA requires coherence between the pump and the signal beam. Maintaining this coherence over long distances requires either the use of a long-coherence length (narrow bandwidth) laser system or the use of an alternative technique, such as exploiting the inter-pulse coherence of different pulses produced by a mode-locked oscillator. From a spatial point of view, the coherence is maintained for light collected from a flat surface over sub-Rayleigh angular range (a single speckle).
3. *Aperture scaling.* The use of QPA is not restricted to a particular aperture size, as a telescope can be used to adapt the beam size collected by the aperture to the size convenient for QPA operation. This resizing has no effect on the field distribution in the units of normalized angle.
4. *Imaging of complex distributions.* We have restricted our discussion to the classical resolution problem formulated by Helstrom, which is treated by the use of binary hypotheses testing. It is conceivable that a more general template-matching approach could also be used to treat more complex distributions with sub-Rayleigh features, in which case one can speculate that both the distances and the positions of multiple objects could be reconstructed. A more complete and general analysis that goes

significantly beyond the scope of this study is needed to determine the potential of QPA in such more complex situations.

7 Conclusion

QPA is a promising method capable of improving the imaging resolution when applied to classical imaging systems that measure the spatial or the spatial frequency distribution of the signal rather than making the complete measurement of the complex electric field of the incident light. We presented a significantly improved model for light detection in conjunction with QPA and considered strategies for SNR improvement. The most important conclusions are reiterated here:

1. As a result of the dependence of gain on the shape of the incident field distribution, QPA is in principle capable of improving the imaging resolution even when an unsegmented detector is used.
2. When a simple intensity distribution measurement is made, the choice between the spatial and the spatial frequency domain for detection affects the achievable SNR improvement. In a typical imaging scenario, the spatial frequency domain is more suitable.
3. For large-amplitude signals it is optimal to select a small detector segment size to capture the details of the intensity distribution.
4. For weak signals a trade-off between the improved sampling and reduced SNR on each detector segment leads to the optimal choice of detector segment size.

In practice, QPA-enhanced imaging systems have to be optimized for a specific application, but the presented general considerations and design criteria are applicable to typical resolution enhancement problems.

Acknowledgements This material is based upon work supported by the U.S. Department of Energy under award DE-NA0000667.

References

1. S.R.P. Pavani, M.A. Thompson, J.S. Biteen, S.J. Lord, N. Liu, R.J. Twieg, R. Piestun, W.E. Moerner, *Proc. Natl. Acad. Sci. USA* **106**, 2995 (2009)
2. P.T.C. So, H.S. Kwon, C.Y. Dong, *J. Opt. Soc. Am. A* **18**, 2833 (2001)
3. M.G.L. Gustafsson, *Proc. Natl. Acad. Sci. USA* **102**, 13081 (2005)
4. Y. Kuznetsova, A. Neumann, S.R. Brueck, *Opt. Express* **15**, 6651 (2007)
5. S.T. Hess, T.P.K. Girirajan, M.D. Mason, *Biophys. J.* **91**, 4258 (2006)
6. G.M. D'Ariano, C. Macchiavello, N. Sterpi, H.P. Yuen, *Phys. Rev. A* **54**, 4712 (1996)
7. R.S. Bondurant, *Opt. Lett.* **25**, 649 (2000)
8. L.A. Wu, H.J. Kimble, J.L. Hall, H. Wu, *Phys. Rev. Lett.* **57**, 2520 (1986)
9. C.M. Caves, *Phys. Rev. D* **26**, 1817 (1982)
10. Y.C. Yin, D. French, I. Jovanovic, *Opt. Express* **18**, 18471 (2010)
11. I. Jovanovic, D. French, J.C. Walter, R.P. Ratowsky, *J. Opt. Soc. Am. B* **26**, 1169 (2009)
12. D. French, Z. Huang, H.-Y. Pao, I. Jovanovic, *Phys. Lett. A* **373**, 999 (2009)
13. Z. Huang, D. French, H.-Y. Pao, I. Jovanovic, *Phys. Lett. A* **373**, 2894 (2009)
14. Z. Huang, D. French, H.-Y. Pao, I. Jovanovic, *Appl. Phys. B* **102**, 607 (2011)
15. C.W. Helstrom, *IEEE Trans. Inf. Theory* **IT 10**, 275 (1964)